

# Thermoformed Parylene-C Cuff Electrodes for Small Nerve Interfacing

Francisco Zurita, Sebastian Freko, Lukas Hiendlmeier, Fulvia Del Duca, Tanja Groll, Olga Seelbach, Katja Steiger, and Bernhard Wolfrum\*

Peripheral nerve interfacing plays a crucial role in various healthcare applications. Generally, interfacing peripheral nerves results in a compromise between selectivity and invasiveness. In particular, large nerves carry many axonal fibers, which are difficult to address selectively without penetrating the nerve. Higher selectivity without nerve penetration can be achieved by targeting small nerves with extraneural cuff electrodes. However, in practice, small nerves are challenging to interface appropriately. Herein, a new multielectrode device is presented that can selectively interface small nerves (<200  $\mu\text{m}$ ). The device is fabricated using rapid laser-based processing with biocompatible materials such as parylene-C and Pt/Ir alloy. Furthermore, the cuff electrode is prefolded via a stick-and-roll thermoforming process, which simplifies the interfacing procedure. It is shown that the device is capable of selectively stimulating the nerve of a locust *in vivo*. Moreover, the subjects show no increased mortality 2 weeks after the implantation of the device.

## 1. Introduction

Bioelectronics for peripheral nerve interfacing (PNI) is a developing field that has drawn a lot of attention in the last decades for its applicability in healthcare. For instance, vagus nerve stimulation is an already approved clinical treatment for depression<sup>[1]</sup> and epilepsy.<sup>[2]</sup> In addition, hypoglossal nerve stimulators, also known as “tongue pacemakers”, are clinically used in patients suffering from obstructive sleep apnea.<sup>[3]</sup> Moreover, there have been successful clinical trials in humans for the treatment of rheumatoid arthritis<sup>[4]</sup> and Crohn’s disease,<sup>[5]</sup> and its use to treat inflammatory bowel disease<sup>[6]</sup> and obesity<sup>[7]</sup> is currently under investigation. PNI is also a key player in the development of bidirectional neuroprostheses, which will allow

amputees not only to control the movement of the limbs with their minds but also feel through them.<sup>[8,9]</sup>


PNI is normally carried out on the larger nerve trunks of the body, whose size simplifies the electrode manufacturing and interfacing procedures. However, larger nerve trunks comprise several nerve fibers, and their stimulation often elicits unintended neuromodulatory responses.<sup>[10]</sup> Fiber selectivity can be improved using intraneural electrodes that pierce through the nerve tissue to come closer to the axons.<sup>[11–13]</sup> However, this procedure causes trauma to the nerve and triggers a strong foreign body response (FBR), quickly degrading the electrodes’ performance.<sup>[14,15]</sup> In contrast, extraneural electrodes only surround the nerve, which reduces nerve trauma and FBR and makes them more suitable for long-term applications.<sup>[16,17]</sup> Nevertheless, they present reduced spatial selectivity as they interact with the axons from the surface of the nerve.<sup>[18]</sup> Techniques to improve the selectivity in extraneural devices include increasing the number of electrodes<sup>[19]</sup> or using the substrate to reshape the nerve.<sup>[20]</sup>

In contrast to the large nerve trunks, the nerves close to their innervating tissue are smaller and comprise fewer axons. Therefore, interfacing small nerves comes as a complementary technique to increasing the selectivity with extraneural electrodes. However, this technique also brings the additional challenge of successfully wrapping an electrode around a small nerve and achieving appropriate electrical contact while minimizing or avoiding nerve damage during the procedure. In particular, the mechanical attachment to the nerves at reduced dimensions remains a limiting factor, not only from the design point of view

F. Zurita, S. Freko, L. Hiendlmeier, F. Del Duca, B. Wolfrum  
Neuroelectronics  
Munich Institute of Biomedical Engineering  
Department of Electrical Engineering  
School of Computation, Information and Technology  
Technical University of Munich  
Hans-Piloty-Str. 1, 85748 Garching, Germany  
E-mail: bernhard.wolfrum@tum.de

T. Groll, O. Seelbach, K. Steiger  
Institute of Pathology  
School of Medicine  
Technical University of Munich  
Trogerstr. 18, 81675 Munich, Germany

T. Groll, O. Seelbach, K. Steiger  
Comparative Experimental Pathology (CEP)  
School of Medicine  
Technical University of Munich  
Trogerstr. 18, 81675 Munich, Germany

 The ORCID identification number(s) for the author(s) of this article can be found under <https://doi.org/10.1002/anbr.202300102>.

© 2023 The Authors. Advanced NanoBiomed Research published by Wiley-VCH GmbH. This is an open access article under the terms of the Creative Commons Attribution License, which permits use, distribution and reproduction in any medium, provided the original work is properly cited.

DOI: 10.1002/anbr.202300102

but also from the practical implementation. Traditional attachment methods include suturing or buckling the electrode around the nerve, or zip tie-based closing mechanisms, which limits their use to specialized practitioners. In recent years, advances in manufacturing techniques have permitted the design of smaller electrodes suitable for small nerve interfacing.<sup>[19,21–25]</sup>

The advances in fabrication technologies have additionally increased the choice of materials for electrode development. Flexible materials and electronics for PNI are currently preferred<sup>[26–29]</sup> since they adapt better to the shape of the softer nerves.<sup>[30]</sup> Materials like polyimide and parylene are being investigated because of their biocompatibility and chemical stability.<sup>[31–34]</sup> Because of these benefits, they have been gaining attention for PNI, for example, in prefolded cuffs.<sup>[33,35–40]</sup> In particular, parylene permits the thermal reshaping of its structure through a process known as “thermoforming”. This process can be leveraged to produce 3D electrode structures, such as helices or cones.<sup>[34,41–43]</sup> Yet, it is challenging to fabricate parylene cuff electrodes for small target nerves (<200 μm) while keeping the handling and implantation procedure as easy as possible.

In this article, we present a multicontact cuff electrode for small nerves. The implemented protocol permits rapid prototyping of the cuff electrodes. The cuffs are prefolded using a stick-and-roll thermoforming process. The process allows precise control of the diameter and opening width so that the cuff can be adjusted to the dimensions of the nerve. Thus, the insertion mechanism reduces to pulling the electrode for the nerve to slide smoothly inside, greatly simplifying the interfacing procedure. Furthermore, the extraction mechanism is simplified as it only involves gently pulling the electrode out. We used parylene-C as a substrate (in the following, also referred to interchangeably as “parylene”) and a Pt/Ir alloy as the electrode material. Furthermore, we confirmed that its implantation in insects does not increase their mortality in the span of 2 weeks. Our device is straightforward to fabricate, as it dispenses with complex and costly lithographic techniques and allows quickly exchanging the metal used, for example, to Pt or Au. Overall, we believe our rapid fabrication process and the cuff design can provide a tool for researchers for in vivo studies on selective nerve stimulation and closed-loop neuromodulation strategies.

## 2. Results and Discussion

### 2.1. Electrode Fabrication

PNI for neuromodulation traditionally targets large nerves. For instance, the sciatic nerve of a rat has a diameter of ≈1 mm and comprises more than 25 000 fibers at the level of the thigh.<sup>[44]</sup> This multitude of fibers makes it challenging to selectively stimulate only the desired fibers without causing off-target responses. Interfacing smaller nerves with fewer fibers intrinsically increases the stimulation selectivity. For this purpose, we developed a small cuff electrode with a straightforward interfacing mechanism. The fabricating procedure is shown in **Figure 1a–g**. We employed thin-film parylene deposition on top of a sacrificial layer for thin-film electrode fabrication. Electrodes and traces were patterned via laser-etching in a rapid prototyping approach. The resulting ≈10 μm-thick parylene

devices are flexible and, therefore, able to accommodate to confined spaces where small nerves are usually found (**Figure 1h,i**). The preformed structures were generated by a thermoforming process. As a consequence, the cuff diameter can be easily adjusted to the desired nerve size (**Figure 1k,l**).

**Figure 2a** shows an optical microscope image of the tip of a 6-electrode device, highlighting an exposed electrode, whereas **Figure 2b** shows a profilometric scan of the highlighted opening. The depth profile was extracted from this scan and showcased in **Figure 2c**, where approximately 5 μm of the top parylene passivation layer was removed, exposing the metallic electrode.

### 2.2. Mechanical Characterization

The mechanical compliance of cuff electrodes to the interfaced tissue is an important characteristic. Since the nerves are in movement with respect to other tissue, the cuff electrodes should be strong enough to remain attached to the nerves under these conditions. However, a very strong compressing force can generate nerve trauma and should be avoided. We estimated the compression force of our devices by measuring the force necessary to open the cuff. The measurement was carried out by attaching the cuff electrodes to a nerve surrogate and pulling it slowly while measuring the force until detachment. For this purpose, we used  $n_{\text{long}} = 16$  devices with a length of  $l_{\text{long}} = 1.6$  mm and  $n_{\text{short}} = 29$  devices with a length of  $l_{\text{short}} = 1.2$  mm and determined that the maximum opening force was below  $F_{\text{open}} = \approx 25$  mN. The obtained low opening force values suggest that the electrode extraction could be performed by simply pulling the electrode off the nerve, which was later experimentally confirmed. Nerve stretching experiments performed in small rodents showed that a force of  $3.25 \pm 0.54$  N is required to break the nerve, and  $0.71 \pm 0.18$  N to abolish compound action potentials.<sup>[45]</sup> Since the opening force values registered for our electrodes were between one and two orders of magnitude lower, we believe our electrodes can be safely applied in vivo in rodents.

### 2.3. Electrochemical Characterization

Characterizing the electrical performance of interfacing electrodes allows for assessing the potential generated upon delivery of a stimulation pulse. This performance is important because high voltages can cause redox reactions, leading to the generation of species that can harm the body. Of particular importance is the electrolysis of water, a process that generates  $\text{H}_2(\text{g})$  and  $\text{O}_2(\text{g})$ . The voltage range in which the electrolysis of water is negligible is commonly called the water window. We carried out cyclic voltammetry (CV) and electrochemical impedance spectroscopy (EIS) to characterize the electrodes. **Figure 3a** shows the resulting averaged voltammograms of 12 electrodes before and after the thermoforming procedure, respectively, which are similar to literature reports on Pt/Ir electrodes.<sup>[46]</sup> In our case, the water window could be safely determined between  $-0.6$  and  $0.8$  V versus Ag/AgCl. The reduction current at around  $0.1$  V is most likely due to oxygen reduction, as pure platinum is well-known to have a pronounced oxygen reduction reaction in this regime under atmospheric oxygen conditions.<sup>[47]</sup> This could

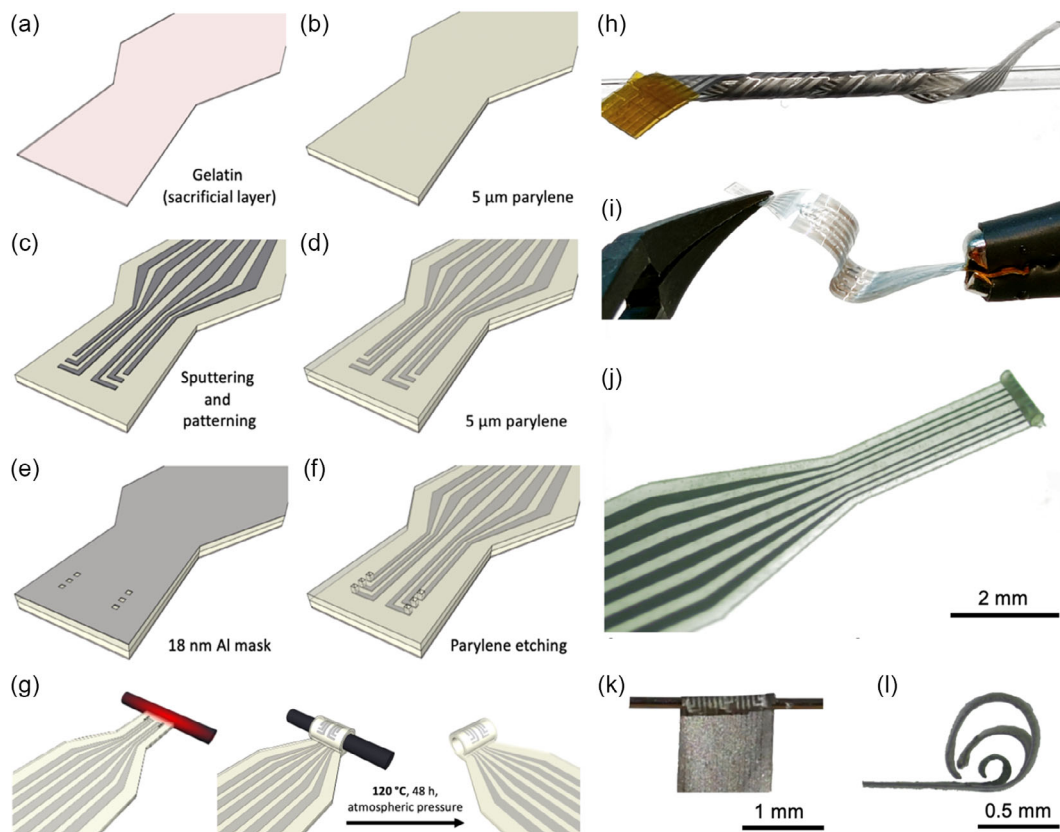


**Figure 1.** Fabrication process of thin-film nerve cuff electrodes and final fabrication results. a) A gelatin layer is spin-coated on a glass slide. b) A parylene layer of 5  $\mu\text{m}$  is deposited on the gelatin. c) 100 nm of Pt/Ir are sputtered on the parylene layer and laser-patterned. d) A second 5- $\mu\text{m}$  parylene layer is deposited. e) An Al mask is sputtered and laser-etched on the desired Pt/Ir electrodes' locations. f) The electrode sites are opened through oxygen etching. g) The tip of the cuff electrode is attached to a resistively heated wire, which is used to roll the cuff ("stick-and-roll"). Afterward, the structure is thermoformed to obtain the final cuff shape. h,i) Electrode wrapped around a glass rod and compression along the neutral axis showing the high flexibility of the electrodes. j) Photograph of a final parylene-based Pt/Ir thin film electrode with 6 feedlines and an inner diameter of approximately 150  $\mu\text{m}$ . k) Image of the electrode attached to a resistively heated wire. l) Overlay of three electrodes with different cuff diameters (150, 300, and 500  $\mu\text{m}$ ).

be prevented by removing the dissolved oxygen in the solution but would not represent experimental conditions.

The cathodic charge storage capacity ( $\text{CSC}_C$ ) was calculated from the measured voltammograms using the following equation:

$$\text{CSC}_C = \frac{1}{\nu A} \int_{E_c}^{E_a} |i_{b,c} - i_{f,c}| dE \quad (1)$$

In this formula,  $\nu$  is the scan rate,  $A$  is the geometric surface area of the electrodes ( $\approx 2500 \mu\text{m}^2$ ),  $E$  is the electrode's potential versus the Ag/AgCl reference electrode,  $i_{b,c}$  is the cathodic part of the current recorded during the backward scan,  $i_{f,c}$  is the cathodic part of the current recorded during the forward scan, and  $E_a$  and  $E_c$  are the anodic and cathodic potential limits, respectively. The average  $\text{CSC}_C$  from  $n = 12$  electrodes decreased from  $5.36 \pm 1.02 \text{ mC cm}^{-2}$  in the unfolded state to  $4.45 \pm 2.76 \text{ mC cm}^{-2}$  in the folded state. A decrease in the  $\text{CSC}_C$  might arise due to the breaking off or splintering of small parts of the metal during the rolling of the thin Pt/Ir layer. This finding is supported by decreased magnitudes of the maximum cathodic and anodic currents in the folded state. The  $\text{CSC}_C$  of the

folded electrodes is in line with literature values for Pt/Ir electrodes with the same atomic ratio (80/20) measured at the same scan rate under aerated conditions.<sup>[48]</sup>

To further characterize the electrochemical properties of our electrodes, we calculated the cathodic charge delivery capacity ( $\text{CDC}_C$ ) from the time integral of the cathodic current, as shown in Figure 3b, using the following formula:

$$\text{CDC}_C = \frac{1}{A} \left| \int_{t_0}^{t_{\text{end}}} i dt \right|, \quad i < 0 \quad (2)$$

where  $A$  is the geometric surface area of the electrodes,  $t_0$  and  $t_{\text{end}}$  represent the starting and ending time of a cycle, respectively, and  $i$  is the measured cathodic current. As expected from the results of the  $\text{CSC}_C$ , the  $\text{CDC}_C$  decreased from  $36.10 \pm 4.96$  to  $27.11 \pm 5.59 \text{ mC cm}^{-2}$  after the thermoforming process. It should be noted that this representation includes faradaic currents, e.g., by the reduction of oxygen. In addition to a possible change in the active electrode area after folding, the geometry of the folded electrode will limit the diffusion of oxygen toward the electrode. This explains the lower magnitude of the reduction

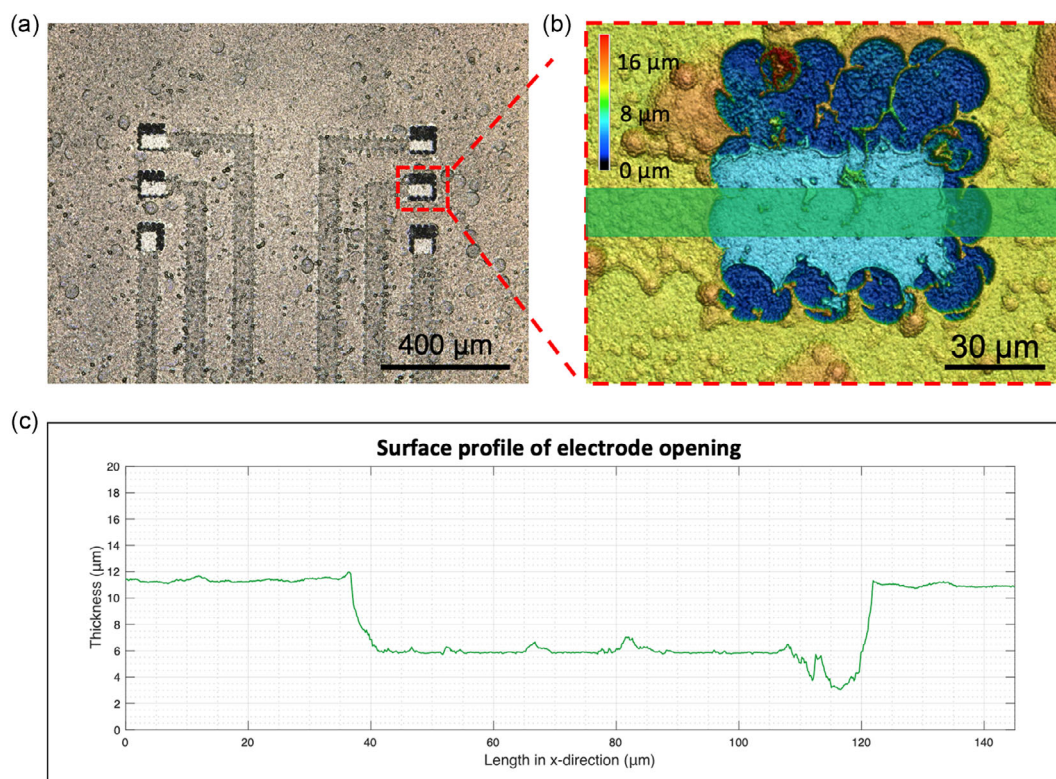


**Figure 2.** Laser etching of the passivation on the electrode sites. a) Microscopic image of electrode tip after the etching process showing the exposed feedlines. b) Magnified height profile of electrode opening. c) Corresponding surface profile, which suggests that the duration of the etching process was sufficient. Parylene residues on the feedline, indicated by small peaks in the height profile, could be explained by inadequate patterning of the Al mask or by O<sub>2</sub> plasma-resistant impurities.

current and the corresponding decrease in charge delivery capacity after thermoforming.

Nerve stimulation involves delivering current through the electrode–electrolyte interface. However, delivering enough current to elicit a nerve response without damaging the electrode is a current challenge for thin-film electrodes.<sup>[49,50]</sup> To make matters worse, thin-film metallic electrodes are prone to delamination.<sup>[51]</sup> Since electrochemical stability is an important characteristic of thin-film electrodes, we applied long-term stimulation and assessed the electrode damage afterward. The long-term stimulation was carried out by delivering short biphasic current pulses with 300 μs pulse width and amplitudes of 100 μA (30 nC), ≈2 times larger than those usually required for stimulation. Figure 3c shows the impedance of  $n = 12$  electrodes before and after applying 10<sup>7</sup> stimulation pulses. It can be seen from Figure 3c that after the long-term stimulation test, some electrodes decreased the mean value of the impedance, probably due to electrode cleaning or delamination of the passivation. Future developments should be directed at improving the adhesion of the Pt/Ir to the parylene-C by either geometrical patterning or appropriate adhesion layers for long-term applications.<sup>[52,53]</sup> Furthermore, functionalizing the electrode surface to reduce impedance could be beneficial if smaller electrode sizes are required.<sup>[54]</sup> This would reduce the stimulation overpotential and, therefore, allow electrodes to deliver higher current densities within the limits of the water window.

#### 2.4. Implantation Procedure and Stimulation

Nerve cuffs with multiple electrodes can increase the stimulation selectivity to elicit the desired response more precisely with fewer side effects. Targeting small nerves, which usually comprise fewer axons than large ones, further increases the stimulation selectivity. We performed in vivo experiments in the insect *Locusta migratoria* to validate the selectivity properties of our cuff electrodes. We interfaced and stimulated nerve 5 (N5), which projects from the metathoracic ganglion and innervates the hind leg. The surgical procedure details have been explained in our previous work.<sup>[55]</sup>

The N5 is a nerve of around 150 μm in diameter, a size that presents challenges to the interfacing. The mechanical attachment to small nerves is crucial since the stimulation efficiency degrades with the distance between the electrode and the nerve tissue.<sup>[56,57]</sup> This reduction in efficiency happens because the stimulation signal is partially shunted through the electrolyte present in the electrode-nerve gap. Our prefolded design minimizes this gap because it conforms to the shape of the nerve, gently displacing the electrolyte in the gap and minimizing the contact distance. Furthermore, the prerolled design also minimizes the interfacing complexity. The cuff electrode must be positioned below the nerve, and careful upward pulling will cause the nerve to gently slide into the cuff. Slightly moving the cuff does not detach the nerve, giving the practitioner some movement freedom. Pulling the cuff

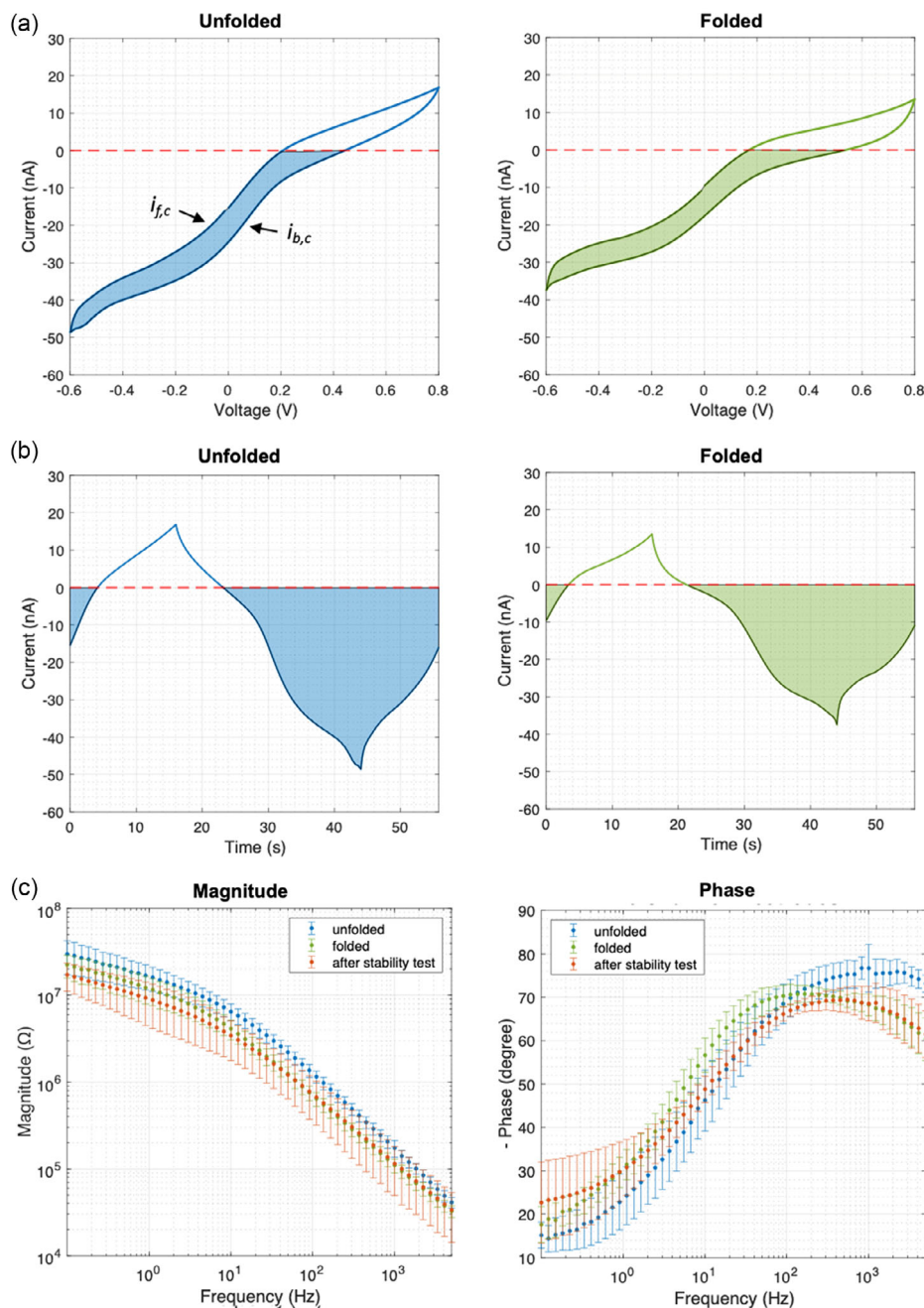


**Figure 3.** Electrochemical characterization of the electrodes. a) Mean of  $n = 12$  voltammograms of the Pt/Ir electrodes versus Ag/AgCl. The water window can then be determined between  $-0.6$  and  $0.8$  V. The colored areas represent the CSC<sub>c</sub> before (unfolded) and after (folded) the thermoforming process. b) Average current over time response of same electrodes ( $n = 12$ ). The colored areas represent the CDC<sub>c</sub>. c) Impedance spectra of the electrodes ( $n = 12$ ) after fabrication (blue), after thermoforming (green), and after aging process (orange). The cots denote mean values and the error bars represent standard deviation.

electrode beyond the opening force stated in the previous section will open the cuff, consequently releasing the nerve. After the extraction, the insect was able to use its leg normally, suggesting that no lasting damage was caused to the nerve by either the interfacing or the extraction procedures.

To assess the electrical performance of the electrodes, we stimulated the N5 under different 1-to-1 electrode combinations and

recorded the elicited leg movement with a camera. The used device comprised 6 electrodes, and all combinations of 2 electrodes without repetitions  $\binom{6}{2} = 15$  were tried. Movement was elicited only in 8 out of the 15 total combinations. Under the same stimulation conditions, no movement was elicited for the other 7 combinations, suggesting that the spatial electrode

configuration plays a role in the selective stimulation of the nerve. **Figure 4e** shows the angle span achieved for every successful electrode combination ( $n = 10$ ). It is important to note that the same experiment in different subjects is not bound to elicit the same results, as there are differences in the relative position between the electrode and the nerve. Therefore, while we observed similar results in other subjects, we reported them only for one subject in this work.

## 2.5. Postimplantation Analysis

To assess the suitability of our devices in insects, we implanted them in 12 locusts and established a control group of also 12 locusts, which only underwent the surgical procedure. Immediately after the surgery, the subjects resumed their regular

activities. Furthermore, they retained their jumping ability, suggesting that the implantation process did not affect the physiology of the nerve. The subjects were kept in their terrarium and observed during the following 2 weeks, under controlled temperature and light patterns. All the subjects in the implanted and control groups survived past the 2 weeks and did not show any impaired behavior or movement patterns, suggesting that our devices do not cause mortality of the subjects within the duration of the experiment.

Next, we histologically evaluated the microscopical location and morphology of the implants in the locusts' body. Samples were fixed in formalin, decalcified, dehydrated, and embedded in paraffin blocks. Hematoxylin-eosin (HE) (**Figure 5**) staining was performed on  $2\ \mu\text{m}$ -sections according to a standard protocol. It should be noted that the cuff electrode shown in **Figure 5a**

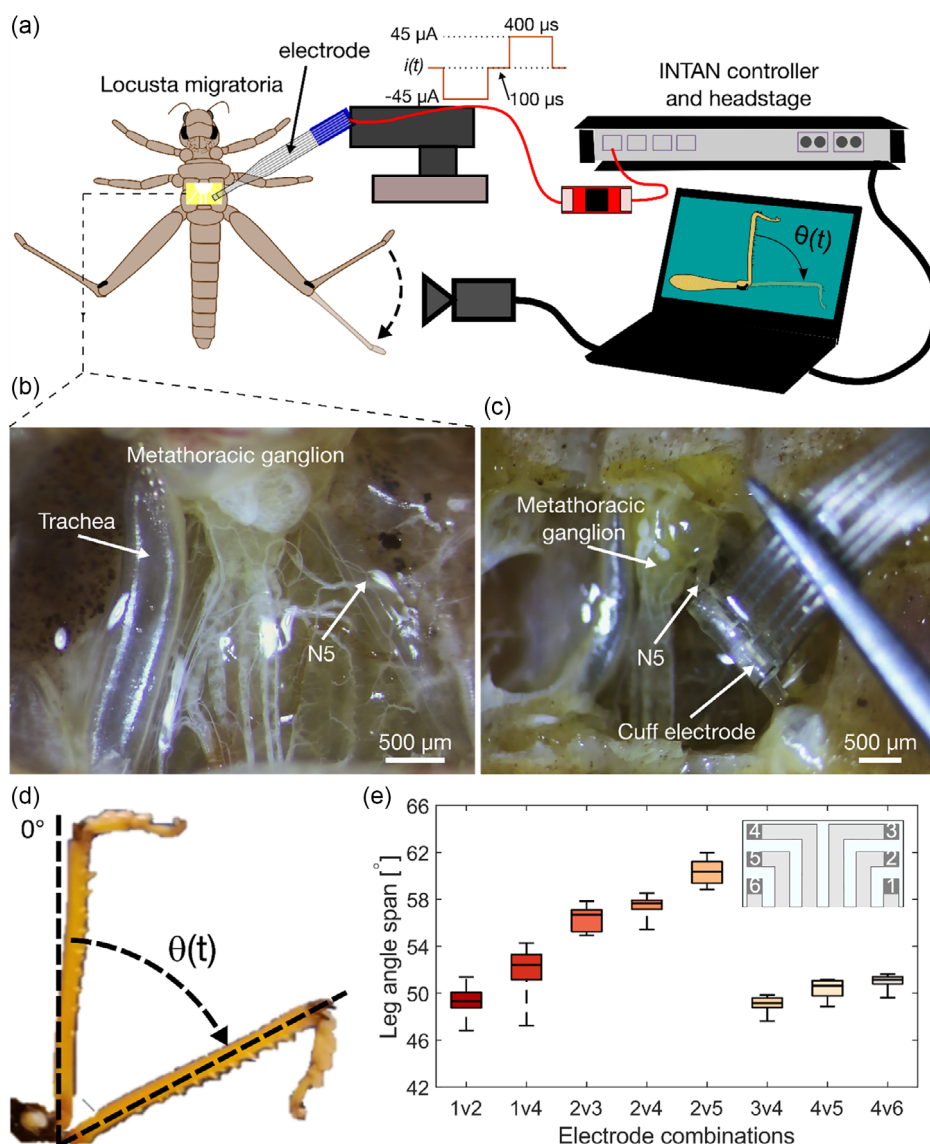


**Figure 4.** a) Schematic of the setup used for in vivo experiments. b) Metathoracic cavity of the locust prior to electrode interfacing, indicating the target nerve. c) Successful nerve interfacing with our cuff electrode. d) Superimposed hind leg image depicting how the angle is measured. e) Angle span for the electrode combinations that elicited leg movement. The inset illustrates the location of the electrode number on the unrolled cuff.

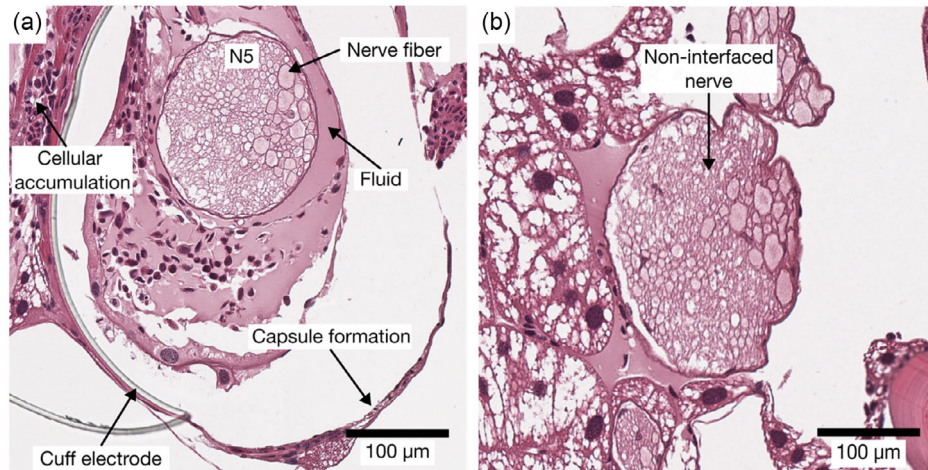


**Figure 5.** a) Histological image of the N5 interfaced with the presented cuff electrodes stained with HE. A monocellular capsule is formed around the parylene-C cuff. The nerve is surrounded by protein-rich fluid containing mononuclear cells. b) A noninterfaced nerve does not present capsule formation and enrichment of cellular fluid around it.

has partially been displaced during the fixation process. Minimal tissue shrinkage appears as a result of tissue fixation. Consequently, in the image, the cuff electrode appears detached from the nerve. However, during insertion, the cuff, which had been tuned to an approximate diameter of 150 µm, closed around the nerve. The images show the formation of a monocellular capsule surrounding the cuff electrodes (Figure 5a), which is not present around nerves that were not interfaced (Figure 5b). The observable reaction is consistent with the physiological encapsulation process of foreign objects in our chosen locust species, as described previously by Brehélin et al.<sup>[58]</sup> Within the capsule and surrounding the nerve, there is a moderately increased accumulation of protein-rich fluid (hemolymph) containing multiple nucleated cells, which are also present adjacent to the mono-layered capsule.

### 3. Conclusion

In this work, we presented a multisite cuff electrode for interfacing small nerves of diameters below 200 µm. The device is pre-folded to the size of the nerve that permits rapid implantation. Furthermore, extraction is also simplified to lightly pulling the electrode. Stimulation of the N5 in locusts with specific electrode configurations yielded repeatable tibiofemoral joint angle extension. Implantation for 2 weeks did not cause mortality or impairment of the insects. Further, tissue histology after the survivability period showed an encapsulation response without severe histopathologic damage. We believe this design could be readily adjusted for assessing selective nerve stimulation in mammals.

### 4. Experimental Section

**Electrode Fabrication:** A glass slide was ultrasonicated for 30 min in acetone, 30 min in isopropanol, and rinsed with deionized water to remove dust and impurities. Then, it was pretreated for 20 min in an oxygen plasma oven (FEMTO, Diener electronic GmbH, Ebhausen, Germany)

and 0.8 mL gelatin was spin-coated for 30 s @ 3000 rpm to form a sacrificial layer. A layer of 5 µm parylene (diX C, Daisan Kasei, Tokyo, Japan) was deposited onto the gelatin layer (Plasma Parylene System GmbH, Rosenheim, Germany). Afterward, a 100 nm layer of Pt/Ir was sputtered on top of the parylene layer. A UV laser marker (MD-U1000C, Keyence, Osaka, Japan) was used to directly ablate the metal and form the traces and electrode structures. The laser has a maximum average power output of approximately 3 W (100%) at 40 kHz repetition rate and a marking resolution of 2 µm. The thin metal film was patterned using the parameters listed in Table 1. Next, another 5 µm parylene layer was deposited on top of the electrodes. To improve the adhesion between the two parylene layers, an adhesion promoter was used (Saline A-174, Plasma Parylene System GmbH, Rosenheim, Germany). An Al mask was sputtered on top of the new parylene layer and laser ablated on top of the electrode sites and contact pads. The exposed parylene sites were plasma-etched (PT7100 Plasma Etcher, Bio-Rad, Hercules, USA) for 25 min to expose the Pt/Ir material on the electrode sites and contact pads. Finally, the electrodes were laser-cut into their final shape using the laser parameters, as shown in Table 1, and released by dissolving the gelatin sacrificial layer in deionized water.

**Thermoforming Process:** A ≈10 cm-long wire (62.4 Ω m<sup>-1</sup>) with a diameter of 100 µm was heated above the glass transition temperature of parylene (≈120 °C) by applying a voltage of approximately 3.5–4 V. The tip of the cuff electrode was brought into contact with the hot wire, which adhered to it. After cooling the wire, the parylene was manually rolled around it to form the lumen of the cuff. The cuff electrode and the wire were then attached to a glass slide with polyimide tape. Next, the cuff electrode was put into an oven and annealed at 120 °C for 48 h to thermoform the tip of the electrode into the desired cuff shape. Finally, the device was taken out of the oven and the wire was carefully removed.

**Table 1.** Laser marking parameters for the fabrication of Pt/Ir thin film electrodes.

Parameter	100 nm Pt/Ir	Aluminum mask	Cut to shape
Power [%]	7	4	15
Speed [mm s <sup>-1</sup> ]	1000	2000	500
Frequency [kHz]	50	90	40
Repetitions	5	4	40
Type	Boundary + Fill	Boundary + Fill	Boundaries

**Mechanical Characterization:** The opening force of the cuff electrodes was measured with a tensile tester (Universal Testing Machine 106, TesT GmbH, Germany). A copper wire with a diameter of 150  $\mu\text{m}$  was mounted on a 3D-printed platform and tightened with screws. The cuff electrode was then carefully wrapped around the copper wire. Both the cuff electrode and the base were mounted on the tensile tester and pulled apart from each other slowly at 0.5 mm min<sup>-1</sup>. The increasing force was recorded until the cuff electrode detached from the wire. The maximum force span was computed for each cuff electrode. The cuff lengths were  $l_{\text{short}} = 1.2$  mm for the short and  $l_{\text{long}} = 1.6$  mm for the long designs.

**Electrochemical Characterization:** The electrochemical properties of the electrodes were characterized using CV and EIS. Both CV and EIS were performed in a Faraday cage using locust's saline solution (147 mM NaCl, 10 mM KCl, 4 mM CaCl<sub>2</sub>, 3 mM NaOH, and 10 mM HEPES buffer, Sigma Aldrich, St. Louis, USA)<sup>[59]</sup> at room temperature in a three-electrode setup, a Ag/AgCl (3 M NaCl) reference electrode and a Pt mesh counter electrode. The measurements were carried out with a potentiostat (PalmSens4, PalmSens, Netherlands). Before the measurements, the electrodes were cleaned in 0.2 M H<sub>2</sub>SO<sub>4</sub> by running a CV for 10 cycles within a potential range from -0.2 to 1.5 V at a scan rate of 500 mV s<sup>-1</sup>.

For the CV measurements, the potential was swept between -0.6 and 0.8 V versus Ag/AgCl with a scan rate of 50 mV s<sup>-1</sup> to keep the Pt/Ir electrode within the water window. Three cycles were recorded in every experiment whereby the last cycles were used for the analysis.

The EIS was measured in a frequency range from 0.1 Hz to 5 kHz by applying a sinusoidal signal with an amplitude of 10 mV ( $n = 12$ ). The electrodes were then subject to a long-term stimulation process, consisting of the application of 10<sup>7</sup> biphasic stimulation pulses (100  $\mu\text{A}$  and 300  $\mu\text{s}$  per phase, 1 ms pulse period). The behavior after the long-term stimulation was characterized by recording the EIS.

**In Vivo Experiments:** We used adult female and male locusts (*Locusta migratoria*) for the stimulation experiments. Since the study was conducted exclusively with insects, no special permission is required in Germany. All experiments complied with the German laws for animal welfare ("Deutsches Tierschutzgesetz"). The locusts were anesthetized by cooling them down to  $\approx 2$  °C for 30 min prior to the surgery. Then, they were placed on a modeling clay base ventral side up. The metathorax cuticle and the metathoracic air sacs were removed using a scalpel and tweezers, exposing the N5. Locust's saline solution was applied to the thoracic cavity to prevent the tissue from drying.<sup>[59]</sup> Next, the cuff electrode was approached and the nerve slid into it.

The electrode contact pads were interfaced with a flat cable using conductive tape (ECATT 9703, 3 M, USA), and the other end of the cable was connected to a zero-insertion-force (ZIF) connector (Würth Elektronik GmbH & Co. KG, Germany). The ZIF connector was then interfaced to an INTAN RHS2116 headset, controlled by the INTAN RHX controller (INTAN Technologies, USA). The INTAN system was used to drive the stimulation currents. The stimulation signal consisted of a biphasic pulse of 400  $\mu\text{s}$  and 45  $\mu\text{A}$  per phase, with an inter-pulse delay of 100  $\mu\text{s}$ . The nerve was stimulated every 3 s and the leg movement response was captured on camera. Finally, the tibiofemoral joint angle was estimated using a custom-made code in MATLAB (MATLAB 2022a, MathWorks, USA).

For the biocompatibility experiments, we implanted the cuff electrodes in 12 subjects. The implantation wound was sealed and the subjects were kept in a terrarium at  $\approx 30$  °C and a 12 h light period for 2 weeks. Afterward, the subjects were sacrificed and samples of the metathorax were fixed in 10% neutral buffered formalin and decalcified using a formic acid-based decalcifying solution. 2  $\mu\text{m}$  sections were cut using a rotating microtome (RM2245 Leica Biosystems, Wetzlar, Germany). The sections were then stained with HE and Masson's trichrome following standard procedures. Slides were then scanned in 40 $\times$  magnification using a whole-slide bright-field scanner (Aperio AT2, Leica Biosystems, Wetzlar, Germany).

## Acknowledgements

The authors thank Lennart Weiss for his support with the electrode preparation for the electrochemical characterization, Inola Kopic for her

guidance during the metal sputtering process, Neil Wagstaffe for his advice regarding the histological processing of the locusts, and Heike Aupperle-Lellbach for her support in the evaluation of the histology. The authors acknowledge funding by the Federal Ministry of Education and Research (BMBF) and the Free State of Bavaria under the Excellence Strategy of the Federal Government and the Länder through the ONE MUNICH Project Munich Multiscale Biofabrication and the TUM Innovation Network: NEUROTECH.

Open Access funding enabled and organized by Projekt DEAL.

## Conflict of Interest

The authors declare no conflict of interest.

## Author Contributions

F.Z. and S.F. contributed equally to this work. F.Z., S.F., and B.W. designed the study. S.F. designed, fabricated, and characterized the devices, with support from L.H. and F.D.D. F.Z. conducted the experiments and processed the data. T.G. performed the histological analysis, with support from O.S. and K.S. All authors reviewed the manuscript and provided critical feedback.

## Data Availability Statement

The data that support the findings of this study are available from the corresponding author upon reasonable request.

## Keywords

cuff electrodes, locust implantation, parylene-C, peripheral nerve interface, thermoforming process

Received: August 24, 2023

Revised: November 9, 2023

Published online: December 3, 2023

- [1] J. M. Bottomley, C. LeReun, A. Diamantopoulos, S. Mitchell, B. N. Gaynes, *Compr. Psychiatry* **2020**, *98*, 152156.
- [2] J. Fan, W. Shan, J. Wu, Q. Wang, *CNS Neurosci. Ther.* **2019**, *25*, 1222.
- [3] C. Heiser, A. Steffen, B. Hofauer, R. Mehra, P. J. Strollo, O. M. Vanderveken, J. T. Maurer, *J. Clin. Med.* **2021**, *10*, 2880.
- [4] F. A. Koopman, S. S. Chavan, S. Miljko, S. Grazio, S. Sokolovic, P. R. Schuurman, A. D. Mehta, Y. A. Levine, M. Faltys, R. Zitnik, K. J. Tracey, P. P. Tak, *Proc. Natl. Acad. Sci. U. S. A.* **2016**, *113*, 8284.
- [5] B. Bonaz, V. Sinniger, D. Hoffmann, D. Clarençon, N. Mathieu, C. Dantzer, L. Vercueil, C. Picq, C. Trocmé, P. Faure, J.-L. Cracowski, S. Pellissier, *Neurogastroenterol. Motil.* **2016**, *28*, 948.
- [6] S. C. Payne, J. B. Furness, O. Burns, A. Sedo, T. Hyakumura, R. K. Shepherd, J. B. Fallon, *Front. Neurosci.* **2019**, *13*, 418.
- [7] G. Yao, L. Kang, J. Li, Y. Long, H. Wei, C. A. Ferreira, J. J. Jeffery, Y. Lin, W. Cai, X. Wang, *Nat. Commun.* **2018**, *9*, 5349.
- [8] A. Cutrone, S. Micera, *Adv. Healthcare Mater.* **2019**, *8*, 1801345.
- [9] K. Kim, *Curr. Opin. Biomed. Eng.* **2022**, *21*, 100368.
- [10] S. L. Florence, N. Jain, M. W. Pospichal, P. D. Beck, D. L. Sly, J. H. Kaas, *Nature* **1996**, *381*, 69.
- [11] M. Mueller, C. Boehler, J. Jaeger, M. Asplund, T. Stieglitz, in *2016 38th Annual Int. Conf. IEEE Engineering in Medicine and Biology Society (EMBC)*, IEEE, Orlando, FL **2016**, p. 2798.



- [12] M. Mueller, N. De La Oliva, J. Del Valle, I. Delgado-Martínez, X. Navarro, T. Stieglitz, *J. Neural Eng.* **2017**, *14*, 066016.
- [13] D. Yan, A. A. Jiman, E. C. Bottorff, P. R. Patel, D. Meli, E. J. Welle, D. C. Ratze, L. A. Havton, C. A. Chestek, S. W. P. Kemp, T. M. Bruns, E. Yoon, J. P. Seymour, *Small* **2022**, *18*, 2200311.
- [14] F. Lotti, F. Ranieri, G. Vadalà, L. Zollo, G. Di Pino, *Front. Neurosci.* **2017**, *11*, 497.
- [15] A. F. Renz, A. M. Reichmuth, F. Stauffer, G. Thompson-Steckel, J. Vörös, *J. Neural Eng.* **2018**, *15*, 061001.
- [16] B. P. Christie, M. Freeberg, W. D. Memberg, G. J. C. Pinault, H. A. Hoyen, D. J. Tyler, R. J. Triolo, *J. Neuroeng. Rehabil.* **2017**, *14*, 70.
- [17] C. Günter, J. Delbeke, M. Ortiz-Catalan, *J. Neuroeng. Rehabil.* **2019**, *16*, 13.
- [18] S. Lienemann, J. Zötterman, S. Farnebo, K. Tybrandt, *J. Neural Eng.* **2021**, *18*, 045007.
- [19] M. A. González-González, A. Kanneganti, A. Joshi-Imre, A. G. Hernandez-Reynoso, G. Bendale, R. Modi, M. Ecker, A. Khurram, S. F. Cogan, W. E. Voit, M. I. Romero-Ortega, *Sci. Rep.* **2018**, *8*, 16390.
- [20] D. J. Tyler, D. M. Durand, *IEEE Trans. Neural Syst. Rehabil. Eng.* **2002**, *10*, 294.
- [21] Y. Zhang, N. Zheng, Y. Cao, F. Wang, P. Wang, Y. Ma, B. Lu, G. Hou, Z. Fang, Z. Liang, M. Yue, Y. Li, Y. Chen, J. Fu, J. Wu, T. Xie, X. Feng, *Sci. Adv.* **2019**, *5*, eaaw1066.
- [22] Y. Liu, V. R. Feig, Z. Bao, *Adv. Healthcare Mater.* **2021**, *10*, 2001916.
- [23] B. Llerena Zambrano, A. F. Renz, T. Ruff, S. Lienemann, K. Tybrandt, J. Vörös, J. Lee, *Adv. Healthcare Mater.* **2021**, *10*, 2001397.
- [24] Y. Liang, A. Offenhäusser, S. Ingebrandt, D. Mayer, *Adv. Healthcare Mater.* **2021**, *10*, 2100061.
- [25] C. C. Rowan, O. Graudejus, T. M. Otchy, *Adv. Sci.* **2022**, *9*, 2102945.
- [26] Z. Xiang, S.-C. Yen, S. Sheshadri, J. Wang, S. Lee, Y.-H. Liu, L.-D. Liao, N. V. Thakor, C. Lee, *Adv. Mater.* **2016**, *28*, 4472.
- [27] Y. Chen, N. J. Rommelfanger, A. I. Mahdi, X. Wu, S. T. Keene, A. Obaid, A. Salleo, H. Wang, G. Hong, *Biomaterials* **2021**, *268*, 120559.
- [28] C. J. Bettinger, *Bioelectron. Med.* **2018**, *4*, 6.
- [29] Y. Shi, R. Liu, L. He, H. Feng, Y. Li, Z. Li, *Smart Mater. Med.* **2020**, *1*, 131.
- [30] J. Kim, R. Ghaffari, D.-H. Kim, *Nat. Biomed. Eng.* **2017**, *1*, 0049.
- [31] T. M. Otchy, C. Michas, B. Lee, K. Gopalan, V. Nerurkar, J. Gleick, D. Semu, L. Darkwa, B. J. Holinski, D. J. Chew, A. E. White, T. J. Gardner, *Nat. Commun.* **2020**, *11*, 4191.
- [32] A. M. Cobo, C. E. Larson, K. Scholten, J. A. Miranda, S. Elyahoodayan, D. Song, V. Píkov, E. Meng, *J. Microelectromech. Syst.* **2019**, *28*, 36.
- [33] H. Yu, W. Xiong, H. Zhang, W. Wang, Z. Li, *J. Microelectromech. Syst.* **2014**, *23*, 1025.
- [34] B. J. Kim, E. Meng, *Polym. Adv. Technol.* **2016**, *27*, 564.
- [35] P. Tian, W. Yi, C. Chen, J. Hu, J. Qi, B. Zhang, M. M.-C. Cheng, *Biomed. Microdevices* **2018**, *20*, 21.
- [36] Y. Seki, S. Yamagiwa, Y. Morikawa, H. Sawahata, R. Numano, M. Ishida, T. Kawano, in *2017 IEEE 30th Int. Conf. Micro Electro Mechanical Systems (MEMS)*, IEEE, Las Vegas, NV **2017**, p. 117.
- [37] X. Kang, J.-Q. Liu, H. Tian, B. Yang, Y. Nuli, C. Yang, *J. Microelectromech. Syst.* **2015**, *24*, 319.
- [38] S. H. Lee, J. H. Jung, Y. M. Chae, J.-K. F. Suh, J. Y. Kang, *J. Microchem. Microeng.* **2010**, *20*, 035015.
- [39] T. Sun, T. Tsaava, J. Peragine, C. Crosfield, M. F. Lopez, R. Modi, R. Sharma, C. Li, H. Sohal, E. H. Chang, L. Rieth, *Acta Biomater.* **2023**, *159*, 394.
- [40] T. Stieglitz, M. Schuettler, A. Schneider, E. Valderrama, X. Navarro, *IEEE Trans. Neural Syst. Rehabil. Eng.* **2003**, *11*, 427.
- [41] B. J. Kim, B. Chen, M. Gupta, E. Meng, *J. Microchem. Microeng.* **2014**, *24*, 065003.
- [42] B. Thielen, E. Meng, *J. Microchem. Microeng.* **2023**, *33*, 095007.
- [43] B. J. Kim, J. T. W. Kuo, S. A. Hara, C. D. Lee, L. Yu, C. A. Gutierrez, T. Q. Hoang, V. Píkov, E. Meng, *J. Neural Eng.* **2013**, *10*, 045002.
- [44] H. Schmalbruch, *Anat. Rec.* **1986**, *215*, 71.
- [45] M. Stecker, K. Baylor, J. Wolfe, M. Stevenson, *J. Brachial Plex. Peripher. Nerve Inj.* **2011**, *06*, e11.
- [46] L. Lu, X. Fu, Y. Liew, Y. Zhang, S. Zhao, Z. Xu, J. Zhao, D. Li, Q. Li, G. B. Stanley, X. Duan, *Nano Lett.* **2019**, *19*, 1577.
- [47] J. Ehlich, L. Migliaccio, I. Sahalianov, M. Nikić, J. Brodský, I. Gablech, X. T. Vu, S. Ingebrandt, E. D. Głowacki, *J. Neural Eng.* **2022**, *19*, 036045.
- [48] S. F. Cogan, P. R. Troyk, J. Ehrlich, T. D. Plante, *IEEE Trans. Biomed. Eng.* **2005**, *52*, 1612.
- [49] P. Oldroyd, G. G. Malliaras, *Acta Biomater.* **2022**, *139*, 65.
- [50] P. Čvančara, T. Boretius, V. M. López-Álvarez, P. Maciejasz, D. Andreu, S. Raspopovic, F. Petrini, S. Micera, G. Granata, E. Fernandez, P. M. Rossini, K. Yoshida, W. Jensen, J.-L. Divoux, D. Guiraud, X. Navarro, T. Stieglitz, *J. Neural Eng.* **2020**, *17*, 046006.
- [51] C. D. Lee, E. Meng, *Front. Mech. Eng.* **2015**, *1*, 10.
- [52] C. Hassler, R. P. Von Metzpen, P. Ruther, T. Stieglitz, *J. Biomed. Mater. Res.* **2010**, *93B*, 266.
- [53] J. Ortigoza-Diaz, K. Scholten, E. Meng, *J. Microelectromech. Syst.* **2018**, *27*, 874.
- [54] G. Dijk, H. J. Ruigrok, R. P. O'Connor, *Adv. Mater. Interfaces* **2020**, *7*, 2000675.
- [55] F. Zurita, F. Del Duca, T. Teshima, L. Hiendlmeier, M. Gebhardt, H. Luksch, B. Wolfrum, *Sci. Rep.* **2022**, *12*, 10864.
- [56] L. Hiendlmeier, F. Zurita, J. Vogel, F. Del Duca, G. Al Boustani, H. Peng, I. Kopic, M. Nikić, T. F. Teshima, B. Wolfrum, *Adv. Mater.* **2023**, *35*, 2210206.
- [57] F. Zurita, L. Grob, A. Erben, F. Del Duca, H. Clausen-Schaumann, S. Sudhop, O. Hayden, B. Wolfrum, *Adv. Mater. Technol.* **2022**, *8*, 2200989.
- [58] M. Brehélin, J. A. Hoffmann, G. Matz, A. Porte, *Cell Tissue Res.* **1975**, *160*, 283.
- [59] R. M. Robertson, K. E. Spong, P. Srithiphaphirom, *Sci. Rep.* **2017**, *7*, 10297.